9

Applications of Ionic Polymer-Metal Composites: Multiple-DOF Devices Using Soft Actuators and Sensors

M. Konyo[1], S. Tadokoro[2], K. Asaka[3]

[1] Graduate School of Information Science, Tohoku University,
6-6-01 Aramaki Aza Aoba, Aoba-ku, Sendai 980-8579, Japan
konyo@rm.is.tohoku.ac.jp
[2] Graduate School of Information Science, Tohoku University
tadokoro@rm.is.tohoku.ac.jp
[3] Research Institute for Cell Engineering, National Institute of AIST,
1-8-31 Midorigaoka, Ikeda, Osaka, 563-8577, Japan
asaka-kinji@aist.go.jp

9.1 Introduction

The ionic polymer-metal composite (IPMC, which is also known as ICPF[*]) [1, 2] is one of the electroactive polymers that have shown potential for practical applications. IPMC is an electroless plated electroactive polymer (EAP) material that bends when subjected to a voltage across its thickness (see Figure 9.1). IPMC has several attractive EAP characteristics that include:

(1) Low drive voltage is 1.0 – 5.0 V).
(2) Relatively high response (up to several tens of Hertz).
(3) Soft material ($E = 2.2 \times 10^8$ Pa).
(4) Possible to miniaturize (< 1 mm).
(5) Durability to many bending cycles (> 1×10^6 bending cycles).
(6) Can be activated in water or in a wet condition.
(7) Exhibits distributed actuation allowing production of mechanisms with multiple degrees of freedom.

The IPMC generates a relatively small force where a cantilever-shaped actuator ($2 \times 10 \times 0.18$ mm) can generate about 0.6 mN, and therefore its applications need to be scoped accordingly. Some of the applications that were investigated for IPMC include an active catheter system [3, 4], a distributed actuation device [5–7],

[*] Kanno and Tadokoro named the Nafion-Pt composite ICPF (Ionic Conducting Polymer gel Film) in 1992. In the field of robotics, most researchers use the name ICPF, and it is well recognized.

an underwater robot [8], micromanipulators [9, 10], a micropump [11], a face-type actuator [7], a wiper of an asteroid rover [12, 13], and a tactile haptic display for virtual reality [14–17]. The actual number of applications that were considered is still small, but the list is expected to grow in the coming years with the emergence of requirements that account for the limitations while taking advantage of the unique capabilities.

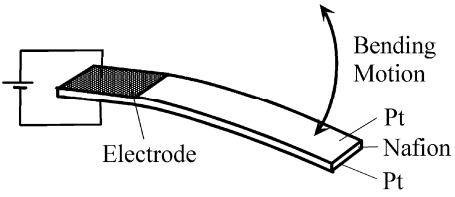

Figure 9.1. Ionic polymer metal composite (IPMC) actuator shown for Pt/Nafion composite EAP

Many investigators have studied models for IPMC, with the largest number addressing Nafion-Pt composite EAP [18–27].

A soft sensing system is also important for advanced applications of IPMC actuators, because conventional solid sensors may cancel the flexibility of an IPMC. One possible sensor would be an IPMC itself. An IPMC can also be used as a sensor, because an electric potential will be generated across the composite when the strip is bent suddenly. The authors showed that the velocity of deformation of an IPMC strip was in proportion to the sensor output voltage and two kinds of velocity-sensing systems were proposed [28]. One is a 3-DOF tactile sensor that has four IPMC sensor modules combined in a cross shape and can detect both the velocity and the direction of the motion of the center tip. Another is a patterned IPMC strip that has both actuator and sensor functions. This strip can sense the velocity of bending motion made by the actuator part.

In this chapter, we describe several robotic applications developed using IPMC materials, which the authors have developed as attractive soft actuators and sensors. In Sections 9.2 to 9.4, several applications of IPMC actuators which have soft actuation mechanisms are described. We introduce several unique applications as follows:

(1) Haptic interface for a virtual tactile display
(2) Distributed actuation device
(3) Soft micromanipulation device with three degrees of freedom

In Section 9.5, we focus on aspects of the sensor function of IPMC materials. The following applications are described:

(1) 3-DOF tactile sensor
(2) Patterned sensor on an IPMC film

9.2. Haptic Interface for Virtual Tactile Display

9.2.1 Background

A novel technology to display to humans more realistic tactile sensation including qualitative information will realize advanced telecommunication directly connected to human physical skills and human mental sensibilities. A cutaneous display in addition to a force display helps human dexterous telemanipulation for use in medicine, space, and other extreme environments. For virtual reality applications, a tactile display is also effective to produce human emotional responses such as a rich texture feel, comfort of touch, and high presence of virtual objects.

A number of tactile displays have been proposed for evoking the cutaneous sense accepted by subcutaneous receptors for rough or frictional feeling on the surface of an object [29]. Conventional mechanical stimulation displays are equipped with a dumbbell-shaped vibration pin, a linear motor, and a pneumatic device. Consequently, it is difficult for the subject to perform contact motion freely in a 3-d space with this type of display due to the weight and size of its actuator .

EAP materials have many attractive characteristics as a soft and light actuator for such a stimulation device. The authors have developed a tactile display using IPMC actuators [14–17]. In our research, the target of tactile information is quite different from conventional ones. Our display can produce a delicate touch including even qualitative information such as a haptic impression or material feel when we stroke the surface of cloth.

The most characteristic feature of tactile sensation is a diversity of perceptual content. This variety is reflected in physical factors of target materials such as rigidity, elasticity, viscosity, friction, and surface shapes. It is interesting that tactile receptors in human skin cannot sense the physical factors directly. They can detect only the inner skin deformations caused by contacting to the objects. This suggests that the reproduction of the same physical factors of materials is not necessary for representing the virtual touch of materials. Virtual touch needs only the reproduction of internal deformations in the skin. Furthermore, a tactile illusion can even be provided by reproduction of nervous activities of tactile receptors, regardless of the inner deformations.

Based on this standpoint, several researchers proposed tactile display methods that make a selective stimulation on each tactile receptor using a magnetic oscillator and air pressure [30] and electrocutaneous stimulation [31]. However, selectivity of stimuli for all kinds of receptors was not enough to reproduce various tactile sensations. By using IMPC actuators, the authors proposed a tactile synthesis method that could control three physical characteristics, which are roughness, softness, and friction, as tunable parameters of textures. This method realizes selective stimulations on each kind of tactile receptors based on its temporal response characteristics [14–17].

In addition, an active perceptual process based on contact motion is very important for human tactile perception. To confirm the feel against hands (haptic impression) people use hand movements consciously or actively to clarify the properties of an object. Such an active touch in connection with contact motion

excels passive sensory perception qualitatively and quantitatively. We successfully developed a wearable tactile display presenting mechanical stimuli on a finger in response to hand movements by using a small interface [16]. Almost no studies had realized a wearable tactile display that could make a multi degree-of-freedom mechanical stimulation on the skin.

In this chapter, haptic interfaces using IPMC actuators are described. Our display can realize a selective stimulation on human skin. We also describe a tactile synthesis method that can control three physical characteristics, which consists of roughness, softness, and friction, as tunable parameters of textures.

9.2.2 Wearable Tactile Display Using ICPF Actuators

Haptic interfaces for presenting human tactile feel were developed using IPMC actuators [14–17]. To express delicate tactile feel including even qualitative information such as tactile impression or material feel, we need to control the sensory fusion of elementary sensations that are generated by different sensory receptors.

Conventional tactile displays could hardly control such delicate sensation because it was difficult to make fine distributed stimuli on a human skin under the limitation of their actuators such as magnetic oscillators, piezoelectric actuators, shapememory alloy actuators, pneumatic devices, and so on. EAP materials have many attractive characteristics as a soft and light actuators for such a stimulation device. IPMC is suitable for the following reasons:

(1) *High spatial resolution*: The required spatial resolution for stimulating sensory receptors, especially Meissner's corpuscle in the finger tip, is less than 2 mm. IPMC films are easy to shape, and their simple operating mechanism allows miniaturizing a stimulator to make a high-density distributed structure. Conventional actuators can hardly control such minute force because of their heavy identical mass and high mechanical impedance. IPMC has enough softness that special control methods are not required to use the passive material property.

(2) *Wide frequency range*: Tactile display can stimulate several tactile receptors selectively by changing frequency ranges because each tactile receptor has different time response characteristics for vibratory stimulation [17]. The required frequency range is from 5 Hz to 200 Hz to stimulate all kinds of tactile receptors. The response speed of IPMC is fast enough to make a vibratory stimulation on a skin higher than 200 Hz. This means that IPMC can stimulate all receptors selectively.

(3) *Stimuli in multiple directions*: Each of the tactile receptors has selectivity for the direction of mechanical stimuli. Meissner's corpuscle detects especially the shearing stress toward the skin surface. Figure 9.2 shows that bending motions of an IPMC, which contacts with a surface of skin in a tilted position, make a stress in both the normal direction and shearing direction.

(4) *Wearability*: In human tactual perception, an active perceptual process based on hand contact motion is very important. To generate the virtual reality of tactile feel, we should move our hand actively and freely, and

receive appropriate stimuli in response to the hand movements. For conventional mechanical stimulation devices of tactile display, it is difficult to attach the device to a finger, so that the subjects cannot perform contact motion freely in a 3-D space. An IPMC based wearable display was successfully developed, which was made so smaller in size and weight that there was no interference with hand movements [16].

(5) *Safety*: The low driving voltage (less than 5 V) is safe enough to touch with a human finger directly.

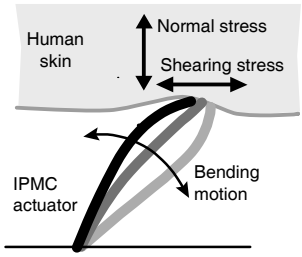

Figure 9.2. Multidirectional stimulation of a human skin using an IPMC actuator

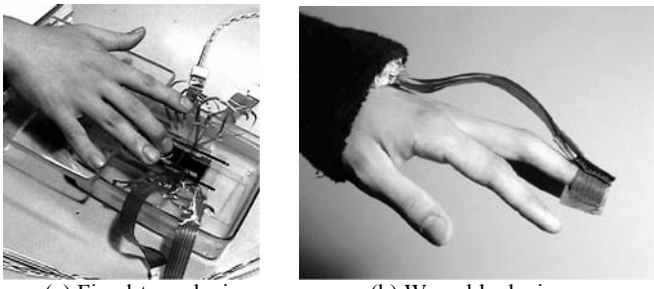

(a) Fixed-type device (b) Wearable device

Figure 9.3. Overview of tactile displays

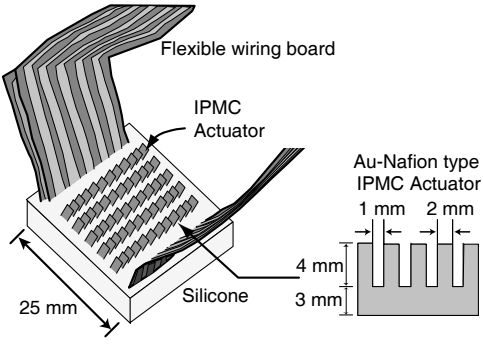

Figure 9.4. Structure of ciliary device using IPMC actuators

In an early prototype [14], tactile feel has been presented as shown in Figure 9.3a. In that case, subjects obtained only passive tactual perception because they could not perform contact motion. As shown in Figure 9.3b, the new wearable device [16] can be attached to the tip of a finger.

The structure of the wearable stimulation device is shown in Figure 9.4. The ciliary part is provided with Nafion-Au composite actuators, where each cilium is 3 mm long and 2 mm wide, in 12 rows leaving 1 mm gaps horizontally and 1.5 mm gaps vertically. All cilia are tilted 45° to transmit mechanical stimuli both in the normal and the tangential directions to the surface of the skin efficiently as shown in Figure 9.2. The power supply line of the IPMC is provided with a flexible wiring board in to minimize restrictions on the hand, so the fingertip can be bent flexibly. The use of silicon rubber of 25 × 25 × 8 [mm] applied to the base of the ciliary part has made it possible to lighten the device to approximately 8 g including the flexible wiring board.

An IPMC needs to be kept moistened because its actuators are operated by ionic migration. Even in a little wet condition in the air, however, the device can provide stimuli sufficiently for several minutes.

Figure 9.5 shows the total display system. The stimulation device is attached to the middle finger tip. The system is designed to read positional information of the hand using Polhemus' FASTRAK, which can read information according to a magnetic field.

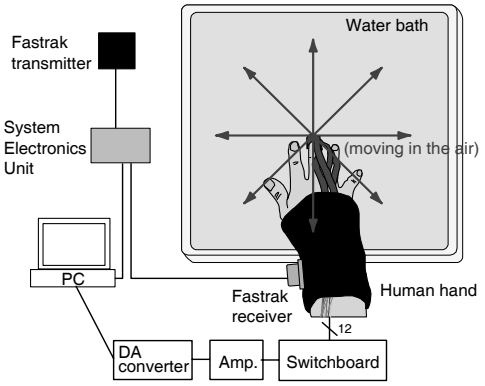

Figure 9.5. Wearable tactile display system in response to virtual contact motion

9.2.3. Concept of the Selective Stimulation Method

In human skin, tactile receptors generate elementary sensations such as touch, pressure, vibratory sensation, pain, temperature sense, and so on. A Tactile impression is an integrated sensation of these elementary sensations. To present tactile feel arbitrarily, stimuli applied to these receptors should be controlled selectively and quantitatively. As mentioned previously, tactile receptors cannot sense the physical factors of environments directly. They detect only the skin deformation caused by contacting objects. A tactile illusion can be provided by reproduction of activities of tactile receptors, regardless of the inner deformations.

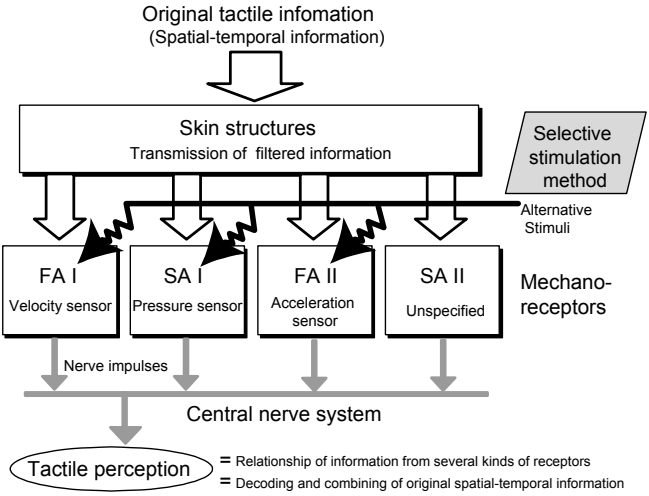

Figure 9.6. Concept of selective stimulation method

Figure 9.6 illustrates the concepts of the selective stimulation method. There are four types of mechanoreceptors embedded in human fingers, FA I type (Meissner's corpuscle), SA I type (Merkel corpuscle), FA II type (Pacinian corpuscle), and SA II type (Ruffini endings) [32]. It is known that each receptor has temporal response characteristics for mechanical stimulation and causes subjective sensation corresponding to its responsive deformation. For example, SA I detects static deformations of skin and produces static pressure sensation, and FA I detects the velocity of the deformation and produces the sense of fluttering vibration. Tactile impression is an integrated sensation of these elementary sensations. To present tactile feel arbitrarily, stimuli applied to these receptors should be controlled selectively.

The first problem is how to stimulate each receptor selectively. We have focused on the frequency response characteristics of tactile receptors. Figure 9.7 [33] illustrates the human detection threshold against vibratory stimuli, which represents the sensibility of each receptor to frequency variation. A smaller amplitude threshold means higher sensibility. This figure shows that there are three frequency ranges in which the most sensitive receptor changes. In the lowest frequency range, SA I is most sensitive relatively. The best becomes FA I in the middle range and FA II in the highest range, respectively. This suggests that the selective stimulation can be realized using these frequency characteristics, and arbitral tactile feels can be produced by synthesizing several frequency components.

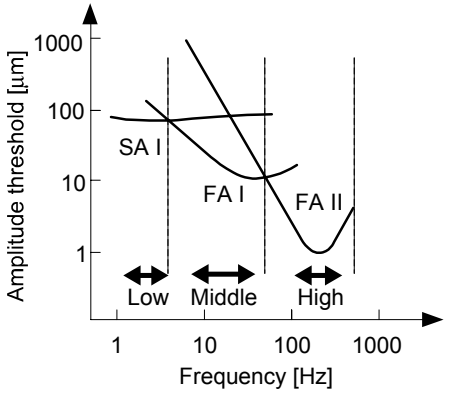

Figure 9.7. Thresholds of tactile receptors for vibratory stimulus and selective stimulation ranges (revised from Maeno [33], which was originally based on Talbot and Johnsson[34] and Freeman *et al.* [35]).

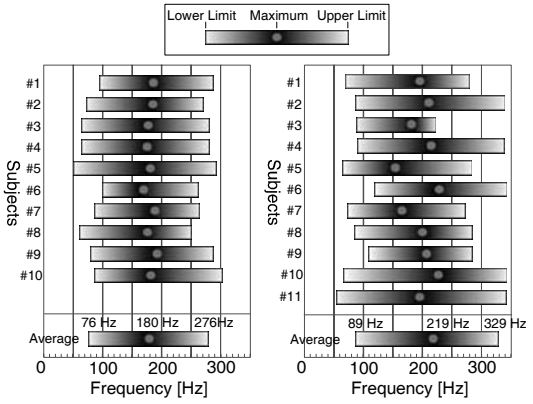

Figure 9.8. Perceptual range of simple vibratory sensation

For the IPMC tactile display, selective stimulation is realized by changing drive frequencies, utilizing the receptors' response characteristics. It was confirmed by subject's introspection that the contents of sensation vary with the change of drive frequency as follows:

(1) *Less than 5 Hz*: static pressure sensation (SA I).
(2) *10 – 100 Hz*: periodical pressing or fluttering sensation, as if the surface of a finger is wiped with some rough material (FA I).
(3) *More than 100 Hz*: simple vibratory sensation (FA II).

Figure 9.8 shows the experimental results of the perceptual range of simple vibratory sensations for (a) fixed-type display and (b) wearable display. It considered that the subjects begin to feel simple vibratory sensation when the

information from FA II exceeds that from FA I. Figure 9.7 shows that the detection threshold of FA II exceeds that of FA I in the vicinity of a frequency from 50 to 100 Hz. This agrees with the results of the perceptual range of vibratory sensation. To create integrated sensations, a stimulating method using composite waves of several frequencies was proposed. Composite waves can stimulate the different kind of tactile receptors at the same time based on the selective stimulation method. In the earlier experiment using the fixed-type IPMC display [14], composite waves of high and low frequencies that present both pressure sensation and vibratory sensation at the same time were applied. The result clearly shows that over 80 % of the ten subjects sensed some special tactile feeling, which is clearly different from a simple vibratory sensation. The authors confirmed that the composite stimulations of two frequency components selected from both the middle and high frequency range illustrated in Figure 9.8 could produce the various qualitative tactile feelings like cloth such as a towel and denim fabric [14].

9.2.4 Texture Synthesis Method

We focused on the following three sensations to produce total textural feeling related to the physical properties of materials: (1) roughness sensation, (2) softness sensation, and (3) friction sensation. These sensations are fundamental to express the textural feel of cloth like materials. The three sensations are produced by the following parameters based on the proposed method described later:

(1) *Roughness sensation:* changes in the frequency and the amplitude caused by the relationship of the wavelength of the desired surface and the hand velocities (Section 9.2.5).
(2) *Softness sensation:* the amount of pressure sensation when the finger contacts the surface (Section 9.2.6).
(3) *Frictional sensation:* changes in the amount of subjective sensation in response to hand accelerations when the finger slides across a surface (Section 9.2.7).

The problem is how to connect the stimulation on each receptor with contact phenomena caused by hand movements and physical properties of objects. We have proposed stimulation methods connected to the relationship between hand movements and the physical properties of objects [17]. For roughness sensation, the frequencies of natural stimuli caused by contacting rough surfaces are changed in response to hand movements. Human beings have the possibility to use those changes of frequencies positively. It is known that the slope of the detection threshold of FA I is –1 in the range of less than 40 Hz, as shown in Figure 9.7. The activities of FA I reflects vibratory frequencies proportionally. This means that FA I can perform as a frequency analyzer in a certain range. Based on this hypothesis, we proposed a frequency modulation method for displaying the roughness sensation in response to hand velocity, as described in the next section.

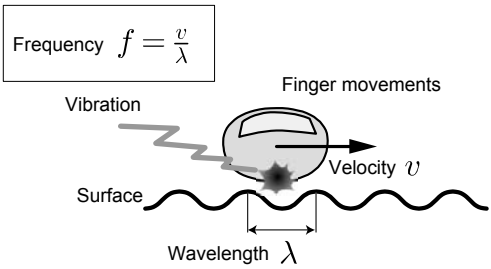

Figure 9.9. Definition of surface form using the wavelength

9.2.5 Display Method for Roughness Sensation

9.2.5.1 Method

As mentioned in Section 9.2.4, we suppose that human beings perceive roughness sensation as the change in frequency detected by FA I in the relationship between their hand movements and the physical properties of the roughness of materials. The roughness of the surface is defined approximately as a sinusoidal surface, which has a given wavelength λ as shown in Figure 9.9. When the finger slides on the sinusoidal surface at a given velocity *v*, the frequency of stimuli *f*, which are generated in a finger point, is expressed by a wave equation as follows.

$$f = \frac{v}{\lambda} \tag{9.1}$$

This equation shows that if the hand velocity becomes faster or if the wavelength λ becomes shorter, the frequency f increases. We should consider the response characteristics of FA I, which is known as a tactile receptor related to the roughness sensation. It is known that FA I respons to the velocity of mechanical stimuli [32]. Here, when the finger slides across the surface, as shown in Figure 9.9, a displacement of stimulus *y* at a given time *t* is defined as a sinusoidal function as follows,

$$y = a\sin(2\pi ft) \tag{9.2}$$

where, *a* is the amplitude of stimulation. Thus, the velocity of stimulation is expressed by substituting Equation (1) in the following equation.

$$\frac{dy}{dt} = 2\pi a\frac{v}{\lambda}\cos(2\pi\frac{v}{\lambda}t) \tag{9.3}$$

This equation presents the information detected by FA I and shows that both the amplitude $2\pi av/\lambda$ and the frequency change in response to the velocity *v*. Based on this assumption, the roughness sensation can be presented by changing both the frequency and the amplitude of stimulation in accordance with hand velocity. In

this manner, the roughness sensation can be defined by the wavelength λ. For practical use of this method, we applied phase adjustments to produce smooth outputs in response to changing frequencies with respect to each sampling time.

Note that these frequencies are just in the high responsive range of FA I. Although the proposed frequency-modulation method is not allowed to apply a suitable range of frequency for FA I explicitly, the appropriate frequencies can be generated by human hand movements consequently, when the wavelength is defined of the order of several millimeters.

9.2.5.2 Evaluations

As evaluation indexes of roughness sensation, nine kinds of close-set lead balls that had different diameters from 0.5 to 10 mm were used as shown in Figure 9.10. The wearable tactile display system shown in Figure 9.5 was used. The amplitudes of stimulations were fixed at 6.0 V (= the maximum input) and each offset was 0.5 V. The offset was needed to avoid an insensitive zone caused by shortage of amplitudes of the actuators.

The subjects put the device on the right middle finger. They touched the index with their left hand at the same time. There was no restriction on time to explore. The subjects were six males in their twenties.

Figure 9.11 shows the relationship between the defined wavelengths and the mean value of selected indexes with each error bar representing one standard deviation. The results showed that as the defined wavelength became longer, the roughness sensation seemed to increase when the two half groups were considered separately. Especially, as the wavelengths became shorter, the standard deviations became smaller and the roughness sensations were expressed clearly.

From the results, it was confirmed that roughness sensation could be expressed by the parameter of the wavelength in the case of relatively short wavelengths. In addition to the wavelength, it is confirmed that the maximum amplitude of stimulus affects the amount of the subjective sensation of roughness.

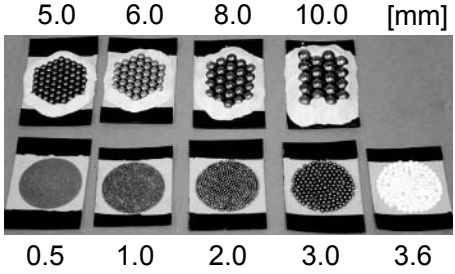

Figure 9.10. Overview of indexes of roughness

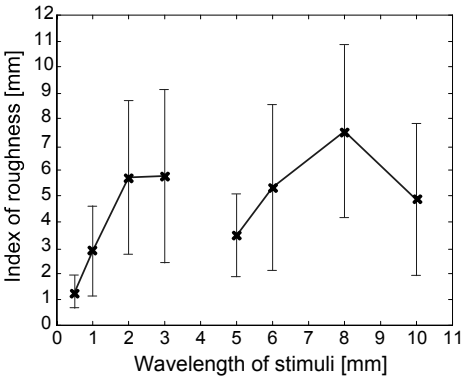

Figure 9.11. Wavelength of stimuli vs. average indexes of roughness sensation

9.2.6. Display Method for Pressure Sensation

9.2.6.1 Method

It is known that SA I detects static deformations of the skin and generates static pressure sensation [32]. Therefore, selective stimulation on SA I can generate pressure sensations. As shown in Figure 9.7, the detection thresholds of SA I hasve flat frequency characteristics in the range of less than 100 Hz. In most of the range of Figure 9.2, FA I is more sensitive than SA I. However, in the range of less than 5 Hz, SA I becomes more sensitive than FA I. This means that the very low frequency vibration can generate pressure sensations relatively larger than the sensation of FA I. The authors confirmed that this assumption was true when the amplitude of simulation was enough small not to sense the vibratory sensation.

9.2.6.2 Evaluations

In this experiment, the wearable tactile display system shown in Figure 9.3b was used. The subjects put the device on the right middle finger. They could perform

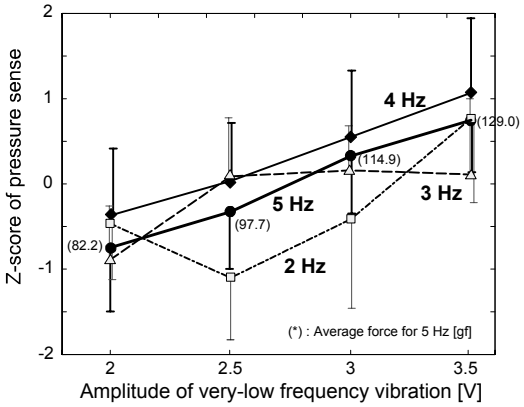

Figure 9.12. Pressure force vs. driving voltage of low-frequency stimulation for SA I

stroke motions in the horizontal direction. The stimulation was simple sinusoidal vibrations at a frequency from 2 to 5 Hz. The stimulations were generated only when the hand velocity was higher than 25 mm/s despite the direction of movement. For measuring pressure sensation, the subjects pushed their left middle finger on a sponge that was set on an electric balance, controlling their finger to the same amount of pressure sensation of the artificial pressure sensation for 3 seconds. And then, the amount of the pressure sensation was calculated as the mean of the force for 3 seconds.

Figure 9.12 shows the relationship between the amplitude of vibration and the amount of pressure sensation at each frequency. The amounts of pressure sensation were calculated by a Z-score because the subjects had different sensitivities for the amount of the subjective sensation. The number in the parenthesis shows the mean value of actual forces at the frequency of 5 Hz as a reference. It was confirmed that as the amplitudes increase, the pressure sensations became larger for every frequency component. Utilizing this method, the softness of materials, which we feel instantaneously when the finger touches a surface, can be expressed by the parameter of amplitude for the frequency components of 5 Hz. If the pressure sensation is larger, the contacting object has more stiffness.

9.2.7 Display Method for Friction Sensation

To express a cloth-like textural feeling in response to contact motions, synthesis of both the roughness sensation and softness sensation is not enough. In this section, we introduce friction sensation. In this study, the definition of friction sensation is not a usual description based on physical contact conditions. We assumed that the friction sensation can be produced as changes in the amount of subjective sensation in response to hand acceleration when the finger slides across the surface. Especially, the friction sensation is used for expressing the sticking tendency of materials at the beginning of sliding motion.

The authors confirmed that stimulation of high-frequency components corresponding to the acceleration of hand movements could produce a natural sliding feeling [16]. It is known that FA II detects the acceleration of stimuli, and it seems that FA II is related to the detection of hand movements such as by a gyro sensor. Figure 9.13 illustrates the relationship between hand acceleration and amplitudes of the high-frequency component. The high-frequency component is fixed at 200 Hz, in which FA II become most sensitive. Therefore, the parameters of the friction sensation are the maximum and minimum values of the amplitude shown in Figure 9.13.

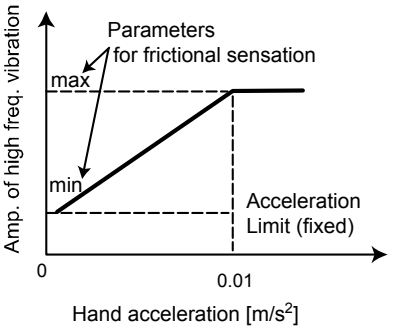

Figure 9.13. Relation between the amplitude of high-frequency components for the friction sensation and the acceleration of hand movements

9.2.8 Synthesis of Total Textural Feeling

9.2.8.1 Method

In this section, syntheses of total textural feeling related to the physical properties of materials based on the three methods described above were evaluated. The voltage inputs generated by the three methods were combined into a signal by a simple superposition. Four materials were selected as targets of the tactile syntheses. The artificial textural feelings were tuned subjectively by changing the parameters of the roughness, softness, and friction sensations. The tunings of textural feelings were extremely easy compared with the author's conventional study because each parameter was related to the physical properties of the materials. The following were the properties of the four materials and the tuned parameters:

(1) *Boa*: shaggy, thick, uneven and very rough surface
($\lambda = 10$, $a = 5.0$, $P = 0.0$, $F_{max} = 2.0$)
(2) *Towel*: rough surface, thick, and soft
($\lambda = 2.0$, $a = 3.0$, $P = 2.0$, $F_{max} = 1.0$)
(3) *Fake leather*: flat surface, thin, hard, and high friction
($\lambda = 8.0$, $a = 1.0$, $P = 4.0$, $F_{max} = 3.0$)
(4) *Fleece*: smooth surface, thin, soft, and low friction
($\lambda = 0.5 = 1.0$, $P = 5.0$, $F_{max} = 1.0$)

9.2.8.2 Evaluations

As shown in Figure 9.14, four artificial textures, which were tuned as mentioned above, were set in a matrix. The four real materials, which were boa, towel, fleece, and fake leather, were put on the cardboard in the same order as the artificial textural feelings. The wearable tactile display system shown in Figure 9.5 was used. The subjects put the device on the right middle or index finger. They could perform stroke motions with their left hand in the horizontal direction. Before the experiments began, the subjects had experience with the four textural feelings only once. The subjects compared each artificial texture with the corresponding real

material. They were to evaluate the similarity of the both feelings at five levels (1: Poor, 2: Fair, 3:Good, 4:Very Good, and 5:Excellent). There was no restriction on time to explore the textures.

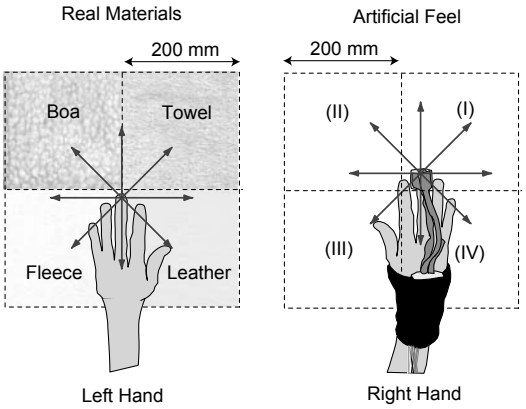

Figure 9.14. Comparison between real materials and artificial tactile feelings

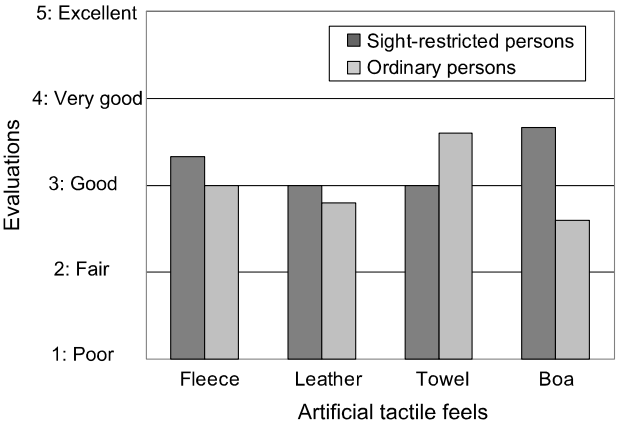

Figure 9.15. Evaluations of artificial tactile feeling compared with the real materials

The subjects were divided into two groups: three sight-restricted people (two females in their fifties and one female in her forties) and five ordinary persons (five males in their twenties). The sight-restricted people have more sensitive tactile sensation than ordinary persons. It was expected that the sight-restricted people could evaluate more correctly.

Figure 9.15 shows the evaluation results for the sight-restricted people and the ordinary persons, respectively. Both of the sight-restricted people and the ordinary

persons judged more than score of 3, that is "Good", for the almost all artificial textures. These results demonstrated that the proposed methods could synthesize the artificial textural feeling corresponding to the real materials. In addition, the sight-restricted people gave higher evaluations than the ordinary persons so that the synthesized textural feelings had the reasonable reality.

Our tactile synthesis method is based on the physical properties of a material. These parameters of textural feeling can be measured as physical properties. This means that the artificial textural feelings could be synthesized automatically, if the tactile sensors could detect such physical parameters. The authors are also developing the tactile transmission system combining the tactile display and tactile sensors as a master-slave system.

9.3. Distributed Actuation Device

The softness of end-effectors is important in manipulation of soft objects like organs, food materials, micro-objects, *etc*. This softness can be actualized using two approaches: (1) drive by hard actuators with soft attachments and (2) direct drive by soft actuators by themselves. The former appears to be a sure method because of present technological development. However, to create micromachines or compact machines like miniature robot hands, the former is limited so it is difficult to find a breakthrough. The problem with the latter is that a readily available soft actuator material does not exist. However, the material revolution currently underway will surely result in the discovery of an appropriate material in the near future. For these reasons, it is meaningful to study methodologies for the effective use of such materials for manipulation with an eye to future applications.

A promising candidate for such a soft actuator material is gel. Many gel materials for actuators have been studied up to the present. The Nafion-platinum composite (IPMC or ICPF) is a new material that is closest to satisfying the requirements for our applications. Because such materials are soft, it is impossible to apply large forces/moments at only a few points on an object, contrary to the case with conventional robot manipulation. At the same time, however, it is an advantage that large pressures cannot be applied actively or passively. So as not to detract from this feature, a number of actuator elements should be distributed for applying the driving force.

The distributed drive is also desirable from the viewpoint of robust manipulation. Even if there are elements that cannot generate appropriate force, in principle, it is possible for the other elements to compensate for them. This signifies insensitivity to environmental fluctuation. In human bodies, for example, excretion of alien substances is performed by a whipping motion of numerous cilia. Paramecia move by paddling their cilia. Centipedes crawl by the cooperative wavy motion of a number of legs. Any of these can robustly accomplish their objectives irrespective of environmental change.

An elliptical friction drive (EFD) element is an actuator element that generates driving force by friction using bending actuators. Figure 9.16 shows an experimental development using the Nafion-Pt composite. It has two actuator parts

with platinum plating for actuation and one Nafion part without plating for an elastic connection. The whole structure is fixed to form the shape of an arch.

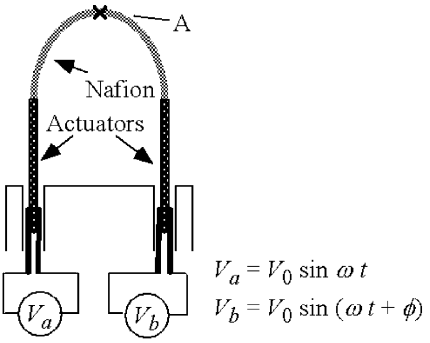

Figure 9.16. Structure of EFD actuator element

When sinusoidal voltages with a phase difference are applied to the two actuators, the excited sinusoidal bending motions also have a phase difference. This results in an elliptical motion at the top point (A) of the connecting part. Figure 9.17 shows a developed distributed EFD device. It has 5 × 8 EFD elements on a plate. They cooperatively apply a driving force to an object.

The driving principle is shown in Figure 9.18. Adjacent elements make elliptical motions with a phase difference of π (a two-phase drive). On the planar contact face, a frictional force in the x direction is generated alternately by adjacent elements, and then the object is driven.

This element could be applied to a robot hand, for example, as shown in Figure 9.19. The Nafion-Pt composite is produced by a process consisting of surface roughening, adsorption of platinum, reduction, and growth on a Nafion membrane. A masking technique using crepe paper tape with a polyethylene coating can be used to form any arbitrary shape of actuator on the Nafion. This technique is called the pattern plating method. It is an essential technique for creating the various shapes in the gel material required for the actuator. It is also important for supplying electricity efficiently.

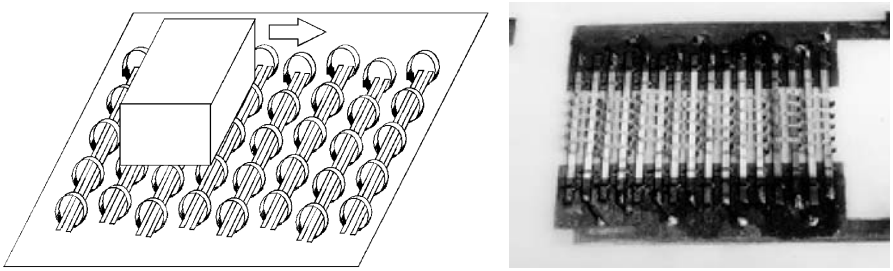

Figure 9.17. Distributed actuation device consisting of multiple EFD elements

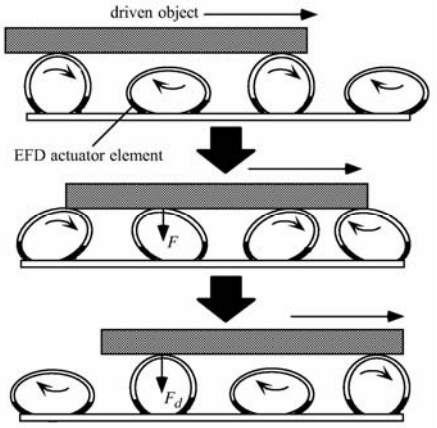

Figure 9.18. Principle of distributed drive

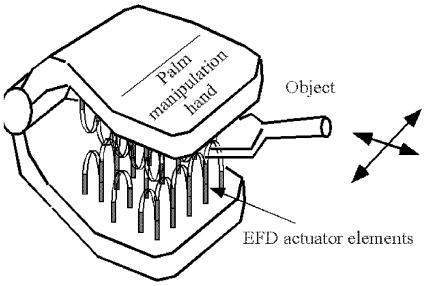

Figure 9.19. Application of device developed as a robotic hand (palm manipulation hand)

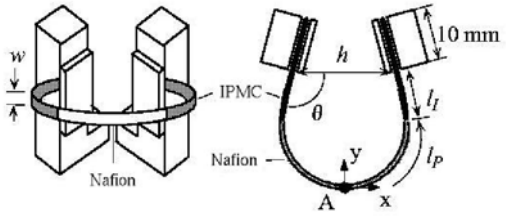

Figure 9.20. Design parameters of EFD element

The manufacturing process is as follows. First, composite actuators are produced on the supports of a Nafion membrane cut in a ladder shape. The ladder is formed into rings by rolling the membrane around a column in a hot water bath. The resultant multiple EFDs are fixed together on a plate. Then, they are wired electrically and the shape of each element is adjusted.

An EFD element has many design parameters of mechanism and control, as shown in Figure 9.20. These parameters have effects on the performance of the element. It is difficult for analytical methods to give an optimal design of these parameters because (1) the actuator part is not a point, (2) the motion of each part

of the actuator is not uniform (output internal stress and time constant), and (3) function of each part interferes each other.

Investigating changing parameters by trial and error, such as in Figure 9.21, is necessary. Models and simulation tools minimize the number of experiments.

The design parameters of the mechanism and control are determined by simulation and analysis using the Kanno-Tadokoro model and an assumption of a viscous friction driving mechanism, as shown in Figure 9.22. The mechanical parameters are listed in Table 9.1.

Figure 9.23 shows the experimental result obtained by varying the phase difference, ϕ, between the sinusoidal input voltages for each EFD element. The shape of the elliptical motion changes according to this phase difference. At the same time, the velocity of the plate changes. Consideration of the analytical and experimental results shows that the elliptical motion in the x direction becomes large when the two phases are similar, and that the y displacement increases when the difference between them is close to π. The speed of the object is determined by these two displacements. The optimal value found in this experiment is $\phi = \pi/2$.

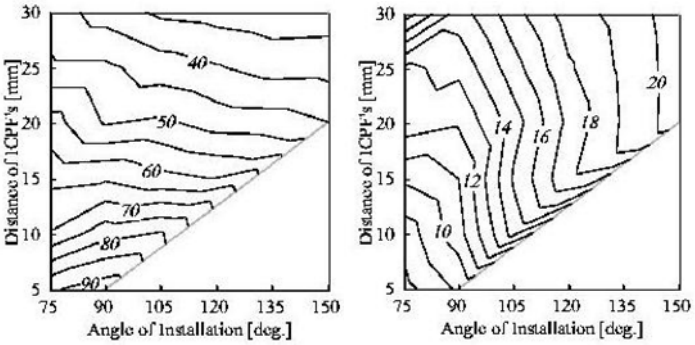

Figure 9.21. Motion of EFD tip vs. design parameters (1 = 62 μm)

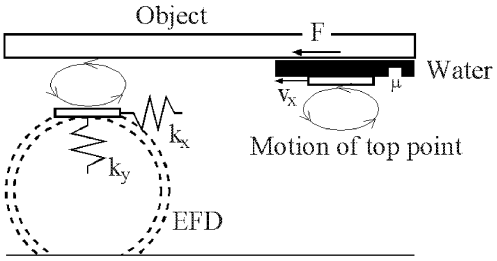

Figure 9.22. Mechanism of distributed drive

Table 9.1. Mechanical design parameters of a distributed device

Parameter	Value
Number of elements (N)	40
Thickness (t)	180 μm
Width (w)	1 mm
Length of ICPF part (l_I)	2 mm
Length of PFS part (l_P)	11 mm
Distance between supports (h)	7 mm
Angle of supports (θ)	180°
Element interval in the x direction (d_x)	14 mm
Element interval in the y direction (d_y)	4 mm

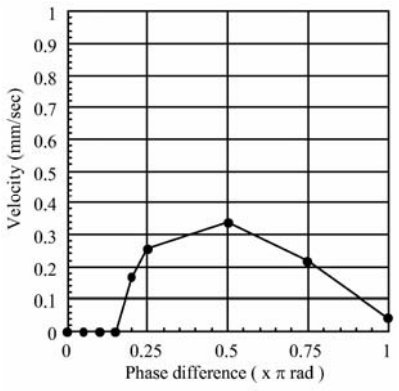

Figure 9.23. Effect of phase difference between the input voltage on the velocity of plate transfer (f = 2 Hz, V_0 = 1.5 V)

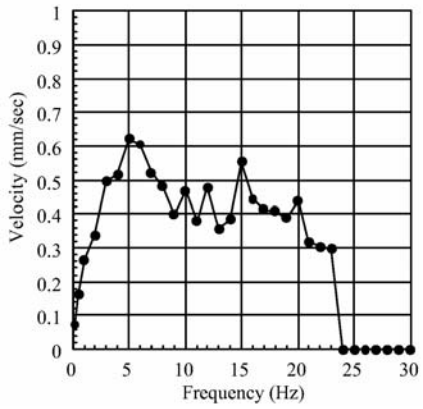

Figure 9.24. Effect of input voltage frequency on the velocity of plate transfer (V_0 = 1.5 V, ϕ = 0.5 π rad)

The results from varying the frequency of the sinusoidal input are shown in Figure 9.24. Analytical results, assuming elasticity of the material, indicate that the resonant frequencies of the element are approximately 5, 10, and 16 Hz. The experimental curve shows good correspondence because the speed is high at these frequencies. The viscous resistance of water is so minor that complex flow near the device can be ignored. The major analysis error results from a modeling error of the contact and the element shape. Under 3 Hz, the experimental result indicates that the velocity increases linearly with frequency. In this range, the speed of the elements is proportional to the frequency because the effect of distributed flexibility is small.

The resonant frequencies vary by 20% depending on the shape of the elements. These frequencies depend on the initial shape and the pressure exerted by the object being manipulated.

9.4. Soft Micromanipulation Device with Three Degrees of Freedom

Micromanipulators require the following elements: (1) compact micro-mechanisms, (2) passive softness, (3) many DOF of motion, and (4) multimodal human feedback. The microactuator is one of the key issues for actualization of such advanced micromanipulators. They are difficult to construct using conventional actuators [36–38].

The important features of the actuators are (1) soft material, (2) force output, (3) ease of miniaturization and machining, and (4) multi-DOF motion ability. A 3-DOF manipulation device is developed by crossing a pair of EFD elements perpendicularly at the end point, as shown in Figure 9.25.

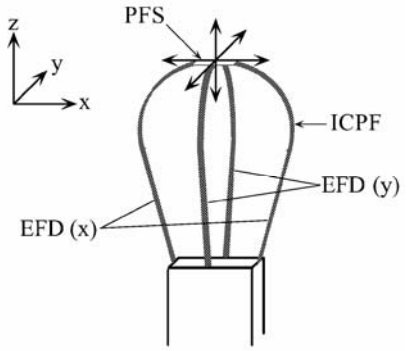

Figure 9.25. Structure of the 3-DOF micromotion device developed

The most important factors in its design are: (1) high flexibility and softness, (2) minimum internal force, and (3) large displacement (especially in 2 DOF). According to a characteristic synthesis using the Kanno-Tadokoro model, the width of the actuator is designed to be as thin as possible (w = 0.4 mm), and the pair of actuators is installed on a fixture in parallel. When external force and

moment $\boldsymbol{f}_i = [f_x, f_y, f_z, n_x, n_y, n_z]^{\mathrm{T}}$ are exerted at the end of the *i*'th actuator segment, They make a minute translation and rotation $\boldsymbol{x}_i = [x, y, z, a_x, a_y, a_z]^{\mathrm{T}}$. The relation is approximated by

$$x_i = C_i f_i, \tag{9.4}$$

where $\boldsymbol{C}_i$ is a compliance matrix. It is a constant matrix if the actuator can be modeled as an elastic body, as in Kanno *et al.* [18]. Considering the viscoelastic property, it becomes a time-varying matrix depending on the deformation history. Because minute translation and rotation of each actuator are expressed by

$$x_i = D_i x_0 \tag{9.5}$$

using the minute motion of the end-effector $\boldsymbol{x}_o$, the force and moment exerted on the end $\boldsymbol{f}_o$ have a relation of a compliance $\boldsymbol{C}_o$ of the end-effector

$$x_0 = C_0 f_0 \tag{9.6}$$

$$C_0 = \left(\sum_i D_i^T C_i^{-1} D_i \right)^{-1}. \tag{9.7}$$

Using an analysis based on the Kanno-Tadokoro model, it was revealed that the developed device was much softer than conventional micromanipulators because the compliance matrix under a static equilibrium condition was

$$C_0 = \begin{bmatrix} 1.9 & 0 & 0 & 0 & 9.3\times10 & 0 \\ 0 & 1.9 & 0 & -9.3\times10 & 0 & 0 \\ 0 & 0 & 3.5\times10^{-1} & 0 & 0 & 0 \\ 0 & -9.3\times10 & 0 & 2.2\times10^{4} & 0 & 0 \\ 9.3\times10 & 0 & 0 & 0 & 2.2\times10^{4} & 0 \\ 0 & 0 & 0 & 0 & 0 & 1.6\times10^{4} \end{bmatrix} \text{ [m/N, rad/Nm]} \tag{9.8}$$

Therefore, this device is safer than a conventional device in manipulation of fragile microstructures. Only the dynamics of the micromanipulator itself were considered here. The actual compliance is affected by surface tension, Van der Waals force, electrostatic force, *etc*. Addressing this issue is beyond the scope of this chapter because these parameters depend on the working environment and cannot be estimated for the manipulator.

Figure 9.26 shows the relation between the magnitude of step input voltage and the resultant maximum displacement. Frequency characteristics under sinusoidal input are shown in Figure 9.27. All experiments in this chapter were performed in water. It was observed that the displacement increases by a quadratic curve

according to the voltage. Displacement in the *z* direction is small because the IPMC (or ICPF) actuators are installed in parallel and this characteristic has been predicted at the stage of design. Displacement in the *xy* direction (diagonal motion in a direction 45° to the *x* axis) is larger than the others because of the effect of the section shape and reduction of internal friction caused by water molecule movement in the material. The maximum displacement observed was 2 mm, and the available frequency range was up to 13 Hz. These performances are sufficient for the micromanipulation application. These characteristics can be predicted by computer simulation using models. In this application, rough estimation was performed using the Kanno-Tadokoro model. However, the accuracy was insufficient to determine the final design.

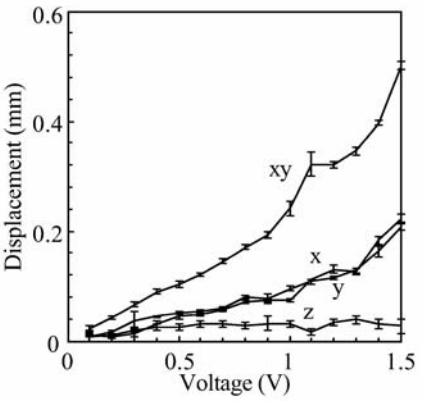

Figure 9.26. Effect of the step input voltage on the displacement

Figure 9.28 illustrates experimental Lissajou figures in the *xy* plane. This demonstrates that the developed device has sufficient motion for micro-manipulation.

The feasibility of telemanipulation by the 3-DOF device was proven using the experimental setup shown in Figure 9.29. Motion commands from an operator are given by a joystick and transmitted to the device via a PC. Actual motion is fed back to the operator by a microscopic image on a monitor. Figure 9.30 is a photographic view of the manipulation setup. The following are revealed as a result of various motion tests:

(1) If the joystick is moved without rest, the device responds to high-speed motion commands completely, and the operator can control the motion very easily.

(2) When the joystick stops, the device does not stop and return to the initial position. The period for which the device could stop at arbitrary points was 3 seconds. The latter characteristic exists because the Nafion-Pt composite material is not a position-type actuator but a force-type actuator.

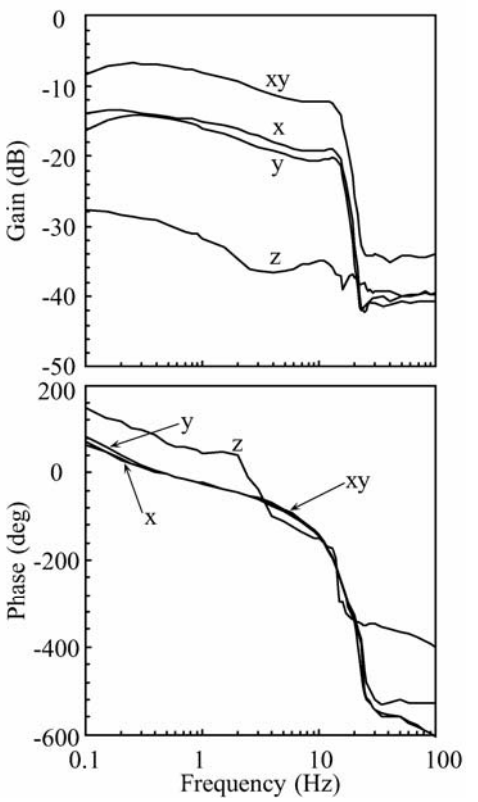

Figure 9.27. Frequency characteristics [input: 1.5 V sinusoidal waves, output: displacement (mm)]

Experiments have shown that the new device is capable of supporting dynamic micromanipulation strategies where dynamic conditions, such as adhesion and pushing, can be major. Gripping or grasping is possible using this manipulator, particularly for short-duration applications that require soft handling. Although effective operation was observed, issues of control still require improvement.

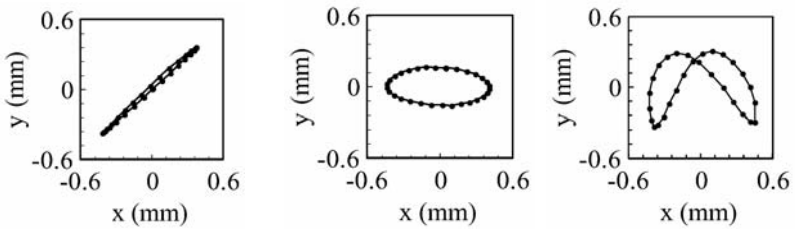

Figure 9.28. Lissajou motion of the 3-DOF device in *xy* plane. (a) $V = 1.5$ V, (b) $\phi = 0.5$, $V = 0.9$, 1.5 V, (c) $f = 1$ Hz and 2 Hz.

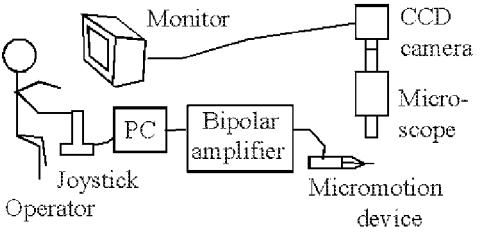

Figure 9.29. Experimental setup for telemanipulation

Figure 9.30. Experiments of direct operator control

9.5 IPMC Sensors

9.5.1 Background

'A soft sensing system is extremely important for advanced applications of IPMC actuators, because conventional solid sensors may cancel the flexibility of IPMC. One possible sensor would be IPMC itself. It was reported that IPMC could be a motion or pressure sensor [39–40], because an electric potential would be generated across the composite when the strip is bent suddenly. Although Shahinpoor *et al.*[39] reported that IPMC sensor output was in proportion to the quasi-static displacement of bending, it is easily confirmed that an IPMC sensor does not respond to static deformation and that there are phase differences between the sensor outputs and the displacements. The authors investigated the relationship between the sensor output and dynamic deformations and showed that the velocity of deformation was in proportion to the sensor output voltage [28].

An IPMC sensor has the following advantages in common with an IPMC actuator's features: (1) Soft material does not cause injury to an object and does not interfere with movements of soft actuators, (2) Light weight and simple structure make device size small.

For example, if an IPMC sensor were used in an active catheter system [3,4], the system could detect contacts with blood vessels without causing injury and could

avoid a critical operational error. Another example is utilization for a tactile display [14–17], as mentioned above. If IPMC sensors were arranged among the vibrators in the same shape and materials, the display system could control the stimulation by measuring the pressure between the ciliary device and the human skin without a negative influence upon tactile feel.

In this manner, a good combination of IPMC sensors and actuators will extend the ability of EAP applications. The following three arrangements can be considered to combine them:

(1) *Switching the sensor/actuator functions*
Both IPMC sensors and actuators can be operated by the same electrodes, if the electric circuits can be switched in two ways. This arrangement seems useful for a system that has many end effectors like a multilegged walking robot.

(2) *Parallel arrangement*
IPMC sensors can be set in parallel with the actuators in order to detect the motion of their body caused by actuation or external disturbances. It is possible to control the actuators based on sensor feedbacks.

(3) *Patterning both functions on an IPMC film*
If an IPMC film is separated electrically by cutting grooves, both the sensor and the actuator can be unified in the same film. This arrangement is more effective to sense motion than the parallel arrangement because there is less interference with the actuation by the sensor part. Using the patterned IPMC cilium, an active sensing system like an insect's feeler can be realized by comparing motion command and sensor feedback.

9.5.2 Basic Characteristics of IPMC Sensor

To investigate the basic characteristics of an IPMC sensor, the relationship between the sensor output and the displacements of vibration were measured, when the IPMC strips were bent by free vibrations. Multiple vibrations with different frequencies were measured by changing the length of an IPMC strip from 8 to 15 mm. The experimental setup is shown in Figure 9.31. A cantilevered IPMC strip was fixed by electrodes. The tip of the strip was hit by the rotary hummer periodically (about 1 Hz) and made a free vibration. An Au-Nafion composite type IPMC [41], which contained the sodium ion, was applied as a sample. The direct-current components of the sensor output are not stable due to the hysteretic influence of previous motion. To avoid the influence, the alternating current components were extracted by a high-pass filter (cutoff frequency: 0.5 Hz), which was set ahead of the amplifier.

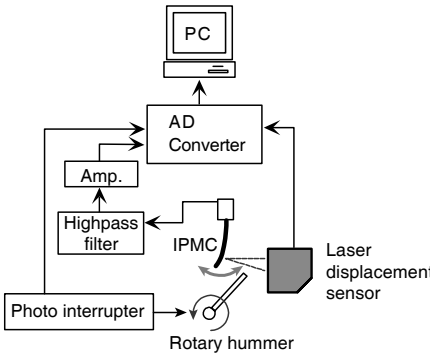

Figure 9.31. Experimental setup

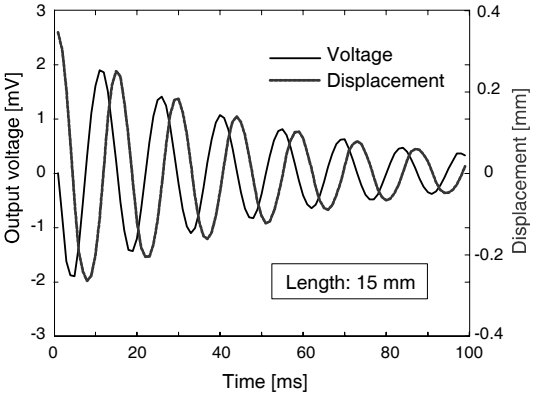

Figure 9.32. Displacements vs. sensor output

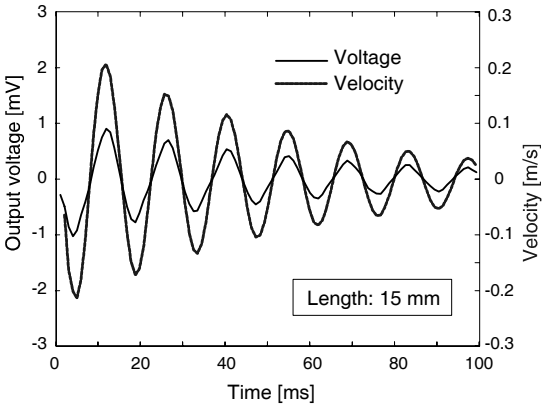

Figure 9.33. Velocities vs. sensor output

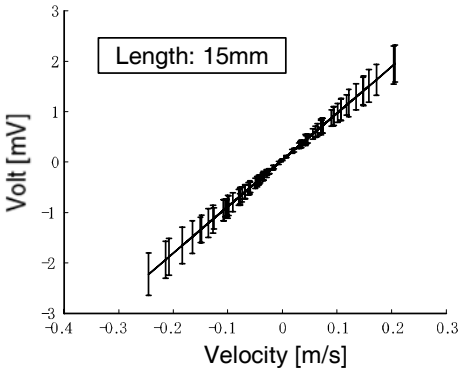

Figure 9.34. The relationship between velocities and sensor outputs

Figure 9.32 shows the example of the relationship between the displacement and the sensor output for the length of 15 mm. The displacements were measured at points 5 mm inside from the free ends.

The outputs were generated in the same frequencies as each free vibration, and the mutual relationship between the amplitude of vibration and that of output was sufficiently estimated from the result of measurement. However, it was confirmed that there the sensor outputs had a phasedelay of approximately 90° toward the displacements. These results suggest that the sensor generates voltages in response to the physical value delayed on the displacement by 90°, that is, the velocity that is given by the differentiation of the displacement.

Figure 9.33 shows the results of the relationship, corresponding to Figure 9.32, between sensor outputs and velocities, which were calculated by the difference of the displacements at each sampling time (1 ms). This figure shows clearly that the phases of the velocity are synchronized exactly with that of the output. Figure 9.33 shows the relationship of the velocities and the sensor outputs on the 15 mm length of IPMC. These results showed that an excellent linear relationship exists between the sensor output and the velocity of bending motion despite the length of the IPMC.

9.5.3 Three-DOF Tactile Sensor

A 3-DOF tactile sensor was developed that has four IPMC sensor modules combined in a cross shape and can detect both the velocity and direction of motion of the center tip. The parallel arrangements of IPMC sensors contribute to the sensing ability to detect a multi degree of freedom and to the improvement of sensing accuracy by error correcting with several outputs. This cross-shape structure of the IPMC was also studied as a 3-DOF manipulator [10]. If the electric circuits could be switched to actuator driving circuits, the 3-DOF tactile sensors would perform as a soft manipulator.

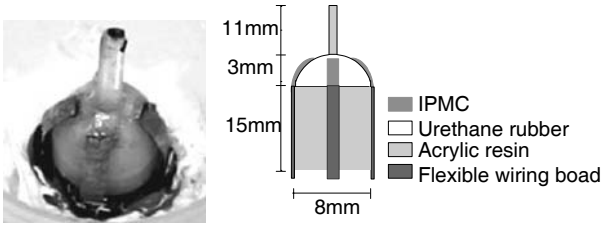

(a) Overview (b) Cross-shape structure

Figure 9.35. The structure of the 3-DOF tactile sensor

Figure 9.36 illustrates the structure of the 3-DOF tactile sensor. Four IPMC strips are combined at the center pole in a cross shape. The center pole is also connected to the domed urethane rubber, which has enough softness and durability and can move in multiple directions. This center pole has the function of extending the deformation of the IPMC strip. To make a quantitative vibratory stimulation, the tip of the center pole was connected to an arm module with a low-adhesiveness bond. The sensor outputs were recorded when the arm module made a sinusoidal motion at several frequencies. The displacements of the tip of the center pole were measured by a laser displacement sensor. In addition, to change in the angle of vibration, the sensor rotated 15° at a time from 0° to 180° as shown in Figure 9.36.

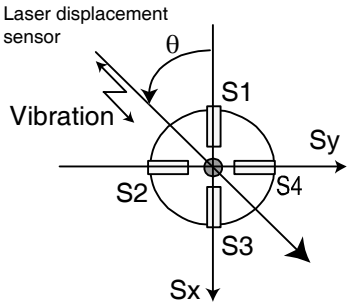

Figure 9.36. Rotational angle of vibratory stimuli

The 3-DOF tactile sensor can detect both the velocity and the direction of motion of the center pole by calculating from the four outputs of the IPMC sensors. The four sensors, however, have individual differences in their outputs, because of individual differences in the IPMC sensor itself and structural differences in the manufacturing process. In this study, the four sensor outputs were calibrated by the mean of the peak-to-peak value of sensor outputs when the rotated angle was 0°. and the frequency was 1 Hz on each sensor.

The direction of motion can be estimated by the relationship of the four sensors. As shown in Figure 9.36, consider two axes of *Sx* and *Sy*, and consider the four sensor outputs are *S1*, *S2*, *S3*, *and S4*. Supposing V_X and V_Y are the components of the the velocity on *Sx* and *Sy*, they can be expressed by the four sensor output as follows

$$V_X = k(S3 - S1) \tag{9.9}$$

$$V_Y = k(S4 - S2) \tag{9.10}$$

where, k is the proportionality constant. Hence, the angle of the motion can be estimated by the relation of V_X and V_Y as follows:

$$V_Y = V_X \tan\theta \tag{9.11}$$

Figure 9.37 shows the comparison between the estimated angle and the theoretical angle by plotting the value of Equation (9.11) and calculating the regression line by the least-squares method for the vibration angles from 0° to 45°. These experimental results show that the estimated angles are in approximate agreement with the theoretical angles.

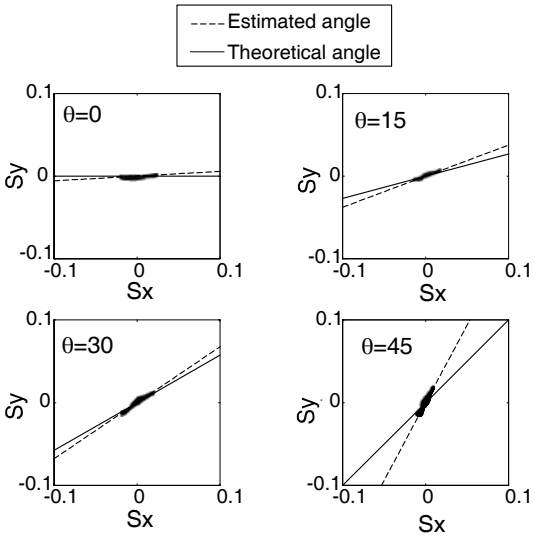

Figure 9.37. Estimated directions of motions

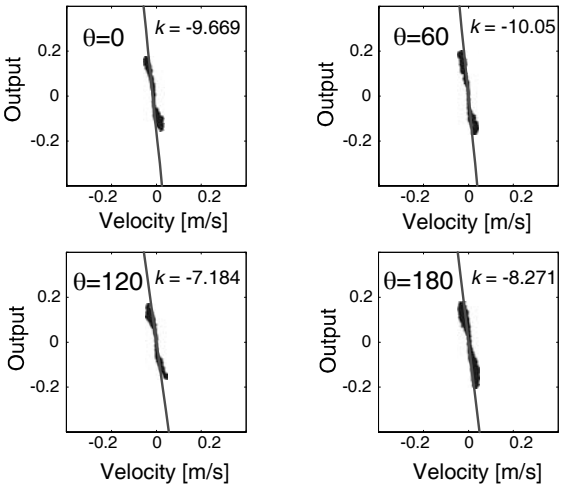

Figure 9.38. Relationship between velocities and the calculated sensor outputs

The velocity of the center pole can also be estimated by the vectors V_X and V_Y. The velocity estimation is calculated separately according to the condition of the angle estimation as follows:

When $0 < \theta < 90$:

$$V = k\left[(S3 - S1)\cos\theta + (S4 - S2)\sin\theta\right] \tag{9.12}$$

When $90 < \theta < 180$:

$$V = k\left[-(S3 - S1)\cos\theta + (S4 - S2)\sin\theta\right] \tag{9.13}$$

Figure 9.38 shows the relationship between the calculated output and the actual velocity calculated from the displacement of the tip of the center pole, where the frequency of vibration is 1 Hz. The proportionality constants k given by the least-squares method are also shown in the figure. The mean and the standard deviation of the proportionality constant k is calculated as follows

$$k = -8.889 \pm 2.185 \tag{9.14}$$

The velocity of the tip of the center pole can be estimated in realtime by using Equations (9.12) and (9.13), the proportionality constant k, and the estimated angle θ.

9.5.4 Patterned Sensor on an IPMC Film

If an IPMC film is separated electrically by cutting grooves, both the sensor and the actuator can be unified in the same film. This arrangement is more effective to sense motion than the parallel arrangement because there is less interference with the actuation by the sensor part.

The authors investigated the possibility of a patterned IPMC strip that had both the actuator and the sensor functions [28]. The strip could sense a velocity of bending motion made by the actuator part. As shown in Figure 9.39 an IPMC strip gave a groove to the depth to be isolated using a cutter for acrylic resin board.

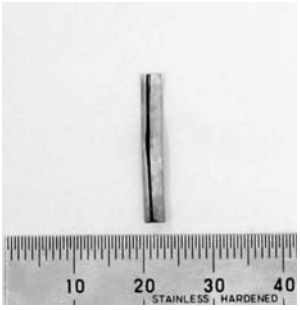

Figure 9.39. Patterned IPMC

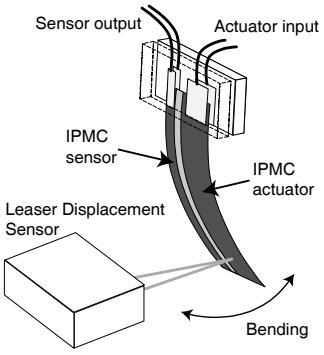

Figure 9.40. Experimental IPMC

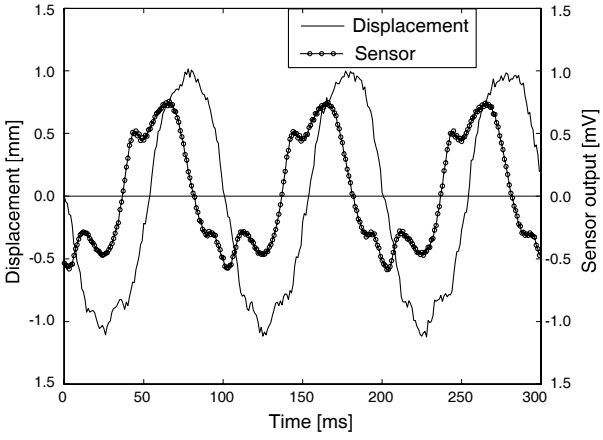

Figure 9.41. Displacement vs. sensor output

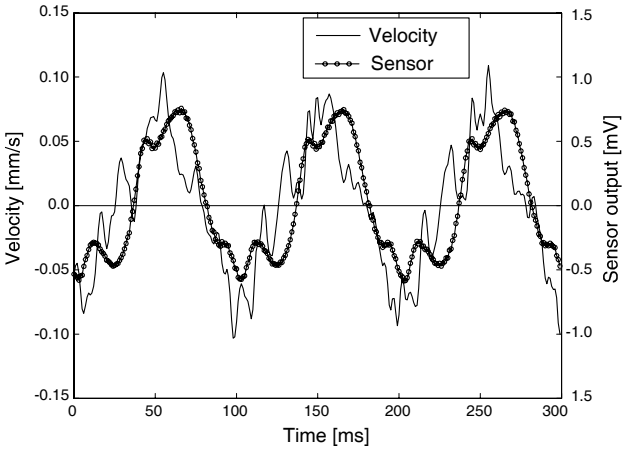

Figure 9.42. Velocity vs. sensor output

The size of the strip is 3 × 20 [mm]. The strip is separated into the two sections, the sensor part is 1 mm wide, and the actuator part is 2 mm wide. The experimental setup is shown in Figure 9.40. Two couples of electrodes were arranged for the actuator and the sensor. The actuator part was driven by a sinusoidal input at a frequency of 10 Hz and in an amplitude of 1.5 V. Displacement of the center of the tip was measured by a laser displacement sensor.

Figure 9.41 shows the relationship between the displacement and the sensor voltage. Figure 9.42 also shows the relationship between the velocity and the sensor voltage. It is clear that the latter agrees more with the sensor output, again. The results demonstrate that a patterned IPMC sensor can detect the velocity of the motion made by the actuator part.

This patterning is a preliminary test to investigate the ability of patterned IPMC. Recently, a patterning technique using laser machining, which can cut a groove of 50 μm wide and about 20 μm deep, was developed by the RIKEN Bio-mimetic Control Research Center team [42]. They have developed a multi-DOF robot using the patterned IPMC actuator. If this technique is utilized for the IPMC sensor, an active sensing system like an insect' s feeler can be realized by comparing a motion command and sensor feedback.

9.6. Conclusions

In this paper, we described several robotic applications developed using IPMC materials, which the authors have been developed as attractive soft actuators and sensors. We introduced following unique devices as applications of IPCM actuators: (1) haptic interface for virtual tactile displays, (2) distributed actuation devices, and (3) a soft micromanipulation device with three degrees of freedom.
We also focused on aspects of sensor function of IPMC materials. The following applications are described: (1)a three-DOF tactile sensor and (2)a patterned sensor on an IPMC film.

9.7 References

[1] Oguro K., Y Kawami, and H. Takenaka, "Bending of an ion-conducting polymer film-electrode composite by an electric stimulus at low voltage," J. of Micromachine Society, Vol. 5, pp. 27-30, 1992.

[2] Shahinpoor M., Conceptual Design, Kinematics and Dynamics of Swimming Robotic Structures using Ionic Polymeric Gel Muscles, Smart Materials and Structures, Vol. 1, No.1, pp.91-94, 1992.

[3] Guo S., T. Fukuda, K. Kosuge, F. Arai, K. Oguro, and M. Negoro, "Micro catheter system with active guide wire," Proc. IEEE International Conference on Robotics and Automation, pp. 79-84, 1995.

[4] Onishi Z., S. Sewa, K. Asaka, N. Fujiwara, and K. Oguro, Bending response of polymer electolete acutator, Proc. SPIE SS-EAPD, pp.121--128, 1999.

[5] Tadokoro S., T. Murakami, S. Fuji, R. Kanno, M. Hattori, and T. Takamori, "An elliptic friction drive element using an ICPF (ionic conducting polymer gel film) actuator," IEEE Control Systems, Vol. 17, No. 3, pp. 60-68, 1997.

[6] Tadokoro S., S. Fuji, M. Fushimi, R. Kanno, T. Kimura, T. Takamori, and K. Oguro, "Development of a distributed actuation device consisting of soft gel actuator elements," Proc. IEEE International Conference on Robotics and Automation, pp. 2155-2160, 1998.

[7] Tadokoro S., S. Fuji, T. Takamori, and K. Oguro, Distributed actuation devices using soft gel actuators, Distributed Manipulation, Kluwer Academic Press, pp. 217-235, 1999.

[8] Guo S., T. Fukuda, N. Kato, and K. Oguro, "Development of underwater microrobot using ICPF actuator," Proc. IEEE International Conference on Robotics and Automation, pp. 1829-1835, 1998.

[9] Tadokoro T., S. Yamagami, M. Ozawa, T. Kimura, T. Takamori, and K. Oguro, "Multi-DOF device for soft micromanipulation consisting of soft gel actuator elements," Proc. IEEE International Conference on Robotics and Automation, pp. 2177-2182, 1999.

[10] Tadokoro S., S. Yamagami, T. Kimura, T. Takamori, and K. Oguro, "Development of a multi-degree-of-freedom micro motion device consisting of soft gel actuators," J. of Robotics and Mechatronics, 2000.

[11] Guo S., S. Hata, K. Sugimoto, T. Fukuda, and K. Oguro, "Development of a new type of capsule micropump," Proc. IEEE International Conference on Robotics and Automation, pp. 2171-2176, 1999.

[12] Bar-Cohen Y., S.P. Leary, K. Oguro, S. Tadokoro, J.S. Harrison, J.G.Smith, and J. Su, "Challenges to the application of IPMC as actuators of planetary mechanisms," Proc. SPIE 7th International Symposium on Smart Structures, Conference on Electro-Active Polymer Actuators and Devices, pp. 140-146, 2000.

[13] Fukuhara M., S. Tadokoro, Y. Bar-Cohen, K. Oguro, and T. Takamori, "A CAE approach in application of Nafion-Pt composite (ICPF) actuators: Analysis for surface wipers of NASA MUSES-CN nanorovers," Proc. SPIE 7th International Symposium on Smart Structures, Conference on Electro-Active Polymer Actuators and Devices, pp. 262-272, 2000.

[14] Konyo M., S. Tadokoro, T. Takamori, and K. Oguro, "Artificial tactile feel display using soft gel actuators," Proc. IEEE International Conference on Robotics and Automation, pp. 3416-3421, 2000.

[15] Konyo M., S. Tadokoro, M. Hira, and T. Takamori, "Quantitative Evaluation of Artificial Tactile Feel Display Integrated with Visual Information", Proc. IEEE International Conference on Intelligent Robotics and Systems, pp. 3060-3065, 2002.

[16] Konyo M., K. Akazawa, S. Tadokoro, and T. Takamori, Wearable Haptic Interface Using ICPF Actuators for Tactile Feel Display in Response to Hand Movements, Journal of Robotics and Mechatronics, Vol. 15, No. 2, pp. 219-226, 2003.
[17] Konyo M., A. Yoshida, S. Tadokoro, and N. Saiwaki, "A tactile synthesis method using multiple frequency vibration for representing virtual touch", IEEE/RSJ International Conference on Intelligent Robots and Systems, pp. 1121-1127, 2005.
[18] Kanno R., A. Kurata, M. Hattori, S. Tadokoro, and T. Takamori, "Characteristics and modeling of ICPF actuator," Proc. Japan-USA Symposium on Flexible Automation, pp. 692-698, 1994.
[19] Kanno R., S. Tadokoro, T. Takamori, M. Hattori, and K. Oguro, "Linear approximate dynamic model of an ICPF (ionic conducting polymer gel film) actuator," Proc. IEEE International Conference on Robotics and Automation, pp. 219-225, 1996.
[20] Kanno R., S. Tadokoro, M. Hattori, T. Takamori, and K. Oguro, "Modeling of ICPF (ionic conducting polymer gel film) actuator, Part 1: Fundamental characteristics and black-box modeling," Trans. of the Japan Society of Mechanical Engineers, Vol. C-62, No. 598, pp. 213-219, 1996(in Japanese).
[21] Kanno R., S. Tadokoro, M. Hattori, T. Takamori, and K. Oguro, "Modeling of ICPF (ionic conducting polymer gel film) actuator, Part 2: Electrical characteristics and linear approximate model," Trans. of the Japan Society of Mechanical Engineers, Vol. C-62, No. 601, pp. 3529-3535, 1996 (in Japanese).
[22] Kanno R., S. Tadokoro, T. Takamori, and K. Oguro, "Modeling of ICPF actuator, Part 3: Considerations of a stress generation function and an approximately linear actuator model," Trans. of the Japan Society of Mechanical Engineers, Vol. C-63, No. 611, pp. 2345-2350, 1997 (in Japanese).
[23] Firoozbakhsh K., M. Shahinpoor, and M. Shavandi, "Mathematical modeling of ionic-interactions and deformation in ionic polymer-metal composite artificial muscles," Proc. SPIE Smart Structure and Material Conference, Proc. SPIE Vol. 3323, pp. 577-587, 1998.
[24] Shahinpoor M., "Active polyelectrolyte gels as electrically controllable artificial muscles and intelligent network structures, Structronic Systems: Smart Structures, Devices and Systems, Part II: Systems and Control," World Scientific, pp. 31-85, 1998.
[25] Tadokoro S., S. Yamagami, T. Takamori, and K. Oguro, "Modeling of Nafion-Pt composite actuators (ICPF) by ionic motion," Proc. SPIE 7th International Symposium on Smart Structures, Conference on Electro-Active Polymer Actuators and Devices, pp. 92-102, 2000.
[26] Tadokoro S., S. Yamagami, T. Takamori, and K. Oguro, "An actuator model of ICPF for robotic applications on the basis of physicochemical hypotheses," Proc. IEEE International Conference on Robotics and Automation, pp. 1340-1346, 2000.
[27] Nemat-Nasser S. and J.Y. Li, "Electromechanical response of ionic polymer metal composites," Proc. SPIE Smart Structures and Materials 2000, Conference on Electro-Active Polymer Actuators and Devices, Vol. 3987, pp. 82-91, 2000.
[28] Konyo M., Y. Konishi, S. Tadokoro, and T. Kishima, Development of Velocity Sensor Using Ionic Polymer-Metal Composites, Proc. SPIE International Symposium on Smart Structures, Conference on Electro-Active Polymer Actuators and Devices, 2003.
[29] Benali-Khoudja M., M. Hafez, J.M. Alexandre, and A. Kheddar, Tactile interfaces: a state-of-the-art survey, 35th International Symposium on Robotics, pp.23-26, 2004.
[30] Shinoda H, N. Asamura, and N. Tomori, A tactile feeling display based on selective stimulation to skin receptors, Proc. IEEE ICRA, pp.435-441,1998.
[31] Kajimoto H, M. Inami, N. Kawakami, and S. Tachi, Smart Touch: Augmentation of Skin Sensation with Electrocutaneous Display, Proc. of the 11th International

Symposium on Haptic Interfaces for Virtual Environment and Teleoperator Systems, pp.40-46, 2003.
[32] Vallbo, Å.B. and Johansson, R.S., Properties of cutaneous mechanoreceptors in the human hand related to touch sensation, Human Neurobiology, 3, pp.3-14, 1984.
[33] Maeno T., Structure and Function of Finger Pad and Tactile Receptors, J. Robot Society of Japan, 18, 6, pp.772-775, 2000 (In Japanese).
[34] Talbot W.H., I. Darian-Smith, H.H. Kornhuber, and V.B. Mountcastle, The Sense of Flutter.Vibration: Comparison of the human Capability with Response Patterns of Mechanoreceptive Afferents from the Monkey Hand, J. Neurophysiology, 31, pp.301-335, 1968.
[35] Freeman A.W., and K.O. Johnson, A Model Accounting for Effects of Vibratory Amplitude on Responses of Cutaneous Mechanoreceptors in Macaque Monkey, J. Physiol., 323, pp.43-64, 1982.
[36] Carrozza M. C., P. Dario, A. Menciassi, and A. Fenu, "Manipulating biological and mechanical micro-objects using LIGA-microfabricated end-effectors," Proc. IEEE International Conference on Robotics and Automation, pp. 1811-1816, 1998.
[37] Ono T., and M. Esashi, "Evanescent-field-controlled nano-pattern transfer and micro-manipulation," Proc. IEEE International Workshop on Micro Electro Mechanical Systems, pp. 488-493, 1998.
[38] Zhou Y., B.J. Nelson, and B. Vikramaditya, "Fusing force and vision feedback for micromanipulation," Proc. IEEE International Conference on Robotics and Automation, pp. 1220-1225, 1998.
[39] Sadeghipour K., R. Salomon, and S. Neogi, Development of a Novel Electrochemically Active Membrane and `Smart' Material Based Vibration Sensor/Damper, Smart Materials and Structures, Vol.1, No.2, pp.172-179, 1992.
[40] Shahinpoor M., Y. Bar-Cohen, J.O. Simpson, and J. Smith, "Ionic polymer-metal composites (IPMC) as biomimetic sensors, Actuators and Artificial Muscles -- A Review," Field Responsive Polymers, American Chemical Society, 1999.
[41] Fujiwara N., K. Asaka, Y. Nishimura, K. Oguro, and E. Torikai, Preparation and gold-solid polymer electrolyte composites as electric stimuli-responsive materials, Chem. Materials, Vol. 12, pp.1750-1754, 2000.
[42] Nakabo Y., T. Mukai, and K. Asaka, A Two-Dimensional Multi-DOF Robot Manipulator with a Patterned Artificial Muscle, Proc. Robotics Symposia, 2004 (In Japanese).